Int. J. Plasma Environ. Sci. Technol. 14 (2020) e01003 (9pp)

International Journal of
Plasma Environmental Science and Technology

Regular Paper

DOI: 10.34343/ijpest.2020.14.e01003

Mechanistic study on nonthermal plasma conversion of CO_2

Dimas Adrianto, Zunrong Sheng, Tomohiro Nozaki *
Department of Mechanical Engineering, Tokyo Institute of Technology, Tokyo, Japan

* Corresponding author: nozaki.t.ab@m.titech.ac.jp (Tomohiro Nozaki)

Received: 14 January 2020
Revised: 7 February 2020
Accepted: 21 February 2020
Published online: 26 February 2020

Abstract

Dielectric barrier discharge (DBD) was generated in a wide range of electric field from 60 to 700 Td by adjusting the operating pressure and the gas gap for the parametric study of electron impact reaction on CO_2 dissociation. Moreover, the effect of specific energy input (*SEI*) was clarified in terms of CO_2 conversion as well as energy efficiency. The results show that CO_2 conversion efficiency increased at higher pressure, while low-pressure operation showed a negligible effect, indicating that generation of vibrational species followed by vibration-to-vibration (V−V) energy transfer, known as ladder-climbing dissociation mechanism, provides a more efficient pathway than electron impact direct CO_2 dissociation reaction. CO_2 conversion increases linearly with *SEI* because energy input per molecule increases. However, energy conversion efficiency decreases by *SEI*, showing a clear trade-off between CO_2 conversion and energy efficiency: such a trade-off relationship is correlated with ladder-climbing dissociation mechanism. Electron impact reaction process was further studied by BOLSIG+, electron Boltzmann equation solver, to gain deep insight into the electronic activation CO_2 in DBD type nonthermal plasma.

Keywords: CO_2 activation, nonthermal plasma, dielectric barrier discharge, vibrational excitation, ladder-climbing dissociation.

1. Introduction

Dielectric barrier discharge (DBD) is among the nonthermal plasmas that acquire a great interest because of possessing a strong nonequilibrium discharge where the electron temperature (1−10 eV; 1 eV = 11,600 K) is substantially higher than gas temperature (ca. 300 K) [1–4]. Moreover, DBD can perform endothermic reactions at ambient temperature and atmospheric pressure [5, 6]. Today, DBD is recognized as an exclusive and effective technology for ozone synthesis [7, 8]. Furthermore, DBD becomes a central subject of research and one of the essential plasma sources in the subject of methane reforming [9–11], carbon dioxides activation [12–14], and N_2 fixation [15, 16]. In CO_2 activation, DBD typically uses a single-step direct electronic excitation mode to dissociate C=O bond. However, the single-step mechanism produces low energy efficiency of less than 15%, which is far from the industrial efficiency of 52% [17]. In contrast, a microwave (MW) plasma, which is also popular for the CO_2 activation, offers a high energy efficiency above 40% by using a vibrational-to-vibrational energy transfer, known as ladder-climbing CO_2 dissociation mechanism [18–20]. The vibrational excitation is known as the influential pathway, which can provide energy efficiency as high as 90% [21]. However, controlling the gas temperature of MW plasma is an important task. As on the increasing gas temperature, a vibrational-to-translational (V−T) relaxation occurs which detriments energy efficiency [17]. Thus, to restrain such V−T deactivation, an operation at a lowered pressure as 120 Torr (16 kPa) is indispensable on MW plasma [22]. Nonetheless, the notable effect of vibrational excitation not only applies to low pressure but also an atmospheric pressure like in gliding arc discharge [23–25]. Gliding arc plasma that uses the same vibrational excitation mode produces a high energy efficiency of 30-40% [26]. However, the trade-off between CO_2 conversion and energy efficiency always confines plasma technology to develop an equally high product yield and energy efficiency [26, 27].

In this study, a DBD reactor was set up to produce a reduced electric field from 60 to 700 Td for initiating vibrational excitation and dissociation collisions of CO_2 activation. The influence of vibrational excitation and dissociation collision of CO_2 activation can be compared and elucidated with DBD, which is difficult with MW plasma. Experimental results show in the electric field of higher than 300 Td, an increase of the dissociation rate constant was negligible to the energy efficiency. In contrast, reducing the electric field from 300 to 60 Td promoted energy efficiency because of an enhancement of the vibrational rate constant. Moreover, electron Boltzmann equation solver (BOLSIG+) was used to estimate electron collision rate constant, showing high pressure and low electric field plasma enhances ladder-climbing CO_2 dissociation mechanism.

2. Experimental

The experiments of CO_2 activation were carried out in a coaxial DBD reactor. The experimental configuration is presented in Fig. 1. A quartz tube was used as a dielectric barrier with the outer and inner diameter of 18 and 15 mm, respectively, providing a dielectric thickness of 1.5 mm. A stainless steel rod was used as an inner electrode and positioned in the center of the quartz tube by O-rings. Four different sizes of the inner electrode, which resulted in four discharge gaps, were used. Detailed parameters of the experiment are shown in Table 1. A stainless steel mesh with length of 70 mm was covered around the outer surface of the quartz tube functioning as a ground electrode. The inner electrode was connected to a high-voltage power source (Logy Electric; LHV-13AC, f = 12 kHz and V_{p-p} = 16 kV maximum, sinusoidal waveform) and the stainless steel mesh (ground) electrode was coupled in series to an external capacitor (33 nF) for charge measurement. Discharge power was calculated by using the Voltage−Charge (Lissajous) diagram. The applied voltage was measured by a high-voltage probe (Tektronix; P6015A), and the charge was measured by a low-voltage probe (RIGOL; PVP2150). All signals were monitored by using a four-channel digital oscilloscope (RIGOL; DS1104B). Feeding gas (CO_2) was sent to the reactor and regulated through a mass flow controller (HORIBA; SEC-E40). Product gaseous elements (CO_2, CO, and O_2) were analyzed online through a quadrupole mass spectrometer (QMS, Prisma-100; Pfeiffer Vacuum GmbH).

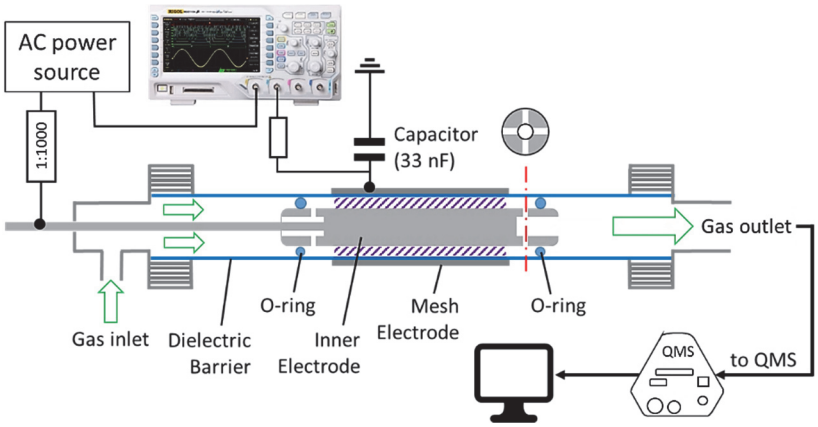

Fig.1. Schematic diagram of the experimental setup.

Specific energy input (*SEI*), CO_2 conversion, and energy efficiency are the essential parameters to evaluate the performance of CO_2 dissociation reaction. The *SEI* expresses the discharge energy consumption per unit volume of the feed gas, which is also interpreted as the mean electrical energy put into a single molecule [28]. Equations 1−3 were used to determine *SEI*, CO_2 conversion, and energy efficiency.

$$SEI\,[\text{eV molecule}^{-1}] = \frac{Power}{N_A\, F_{CO_2}^{in}} \tag{1}$$

$$\chi_{CO_2}\,[-] = \frac{F_{CO_2}^{in} - F_{CO_2}^{out}}{F_{CO_2}^{in}} \tag{2}$$

$$\eta\,[\%] = \frac{\chi_{CO_2}\, N_A\, F_{CO_2}^{in}\, \Delta H_R}{Power} = \frac{\chi_{CO_2}\, \Delta H_R}{SEI} \tag{3}$$

Here, N_A is the Avogadro's number, F and ΔH_R denote mole flow rate of CO_2 (mol s^{-1}) and the reaction enthalpy of CO_2 dissociation, respectively: (ΔH_R = 283 kJ/mol = 2.93 eV/molecule for $CO_2 = CO + 0.5O_2$). The energy efficiency is defined by the endothermic energy of CO_2 dissociation divided by input energy.

Table. 1. Experimental parameters of CO_2 activation

Discharge gap	CO_2 flow rate STP (25 °C − 101 kPa)	Operating pressure
0.5 mm	85 cm^3 min^{-1}	15 kPa
1.5 mm		45 kPa
2.5 mm	400 cm^3 min^{-1}	75 kPa
3.5 mm		

3. Results and discussion

3.1 CO_2 conversion *vs.* energy efficiency: trade-off relationship

Fig. 2 shows the Voltage-Charge (Lissajous) diagram. The BC and DA slopes represent the event of discharge and the charge accumulation period. On the other hand, the AB and CD slopes express the discharge-off condition. Moreover, because the Lissajous diagram is asymmetric, the sustaining voltage of CO_2 was determined by the average value of negative (U_{sus}^-) and positive (U_{sus}^+). Such asymmetricity arises because the power source generates a slightly deformed sinusoidal signal. The reduced electric field (E/N) was varied from 60 to 700 Td by adjusting the pressure as well as discharge gap as formulated by Eq. 4. The reduced electric field is commonly expressed in a unit called Townsend (Td), where 1 Td corresponds to 10^{-21} Vm^2.

$$\frac{E}{N}[Vm^2] = \frac{\bar{U}_{sus}}{\text{discharge gap}} \times \frac{RT}{PN_A} \quad (4)$$

Here, E expresses the electric field acting over the gas gap. The molecule density (N) was estimated from gas temperature and pressure. The R is the gas constant and $\bar{U}_{sus}$ expresses the average discharge sustain voltage which is read from the Lissajous diagram (Fig. 2). The influence of operating pressure, *SEI*, and E/N on CO_2 conversion behavior was investigated.

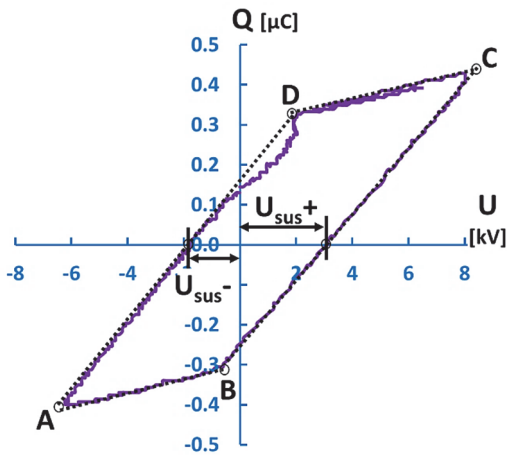

Fig. 2. Lissajous diagram (45 kPa, 44 W,12 kHz).

The effect of pressure on energy efficiency is indicated in Fig. 3. Experimental data is clarified uniquely over the pressure-to-gap matrix as highlighted by the dotted lines. In an electric field from 60 to 300 Td, 75 kPa produced the most significant improvement of energy efficiency, then followed by 45 kPa and 15 kPa. Also, point out that energy efficiency increases with the reduced electric field except for the data for a 0.5 mm gap

at 15 kPa. Based on observation, the higher electric field (up to 300 Td) promotes energy efficiency. Meanwhile, the effect of operating pressure is much greater than that of the reduced electric field. The effect of the gas gap is small at 75 kPa and 45 kPa; the reduced electric field is distributed between a narrow range of 60 and 300 Td by changing the gap from 3.5 mm to 0.5 mm, indicating that discharge property may not change to a large extent in these cases. A similar trend is observed in the case of 15 kPa except for 0.5 mm gap. However, by reducing the gap from 1.5 mm to 0.5 mm, the reduced electric field increases significantly up to 700 Td; correspondingly, the data is off the red line, showing that discharge properties at 15 kPa and 0.5 mm gap is clearly different from other conditions. Due to the high electric field at low gas pressure, the direct dissociation pathway becomes dominant that deteriorates energy efficiency which is further discussed in section 3.2.

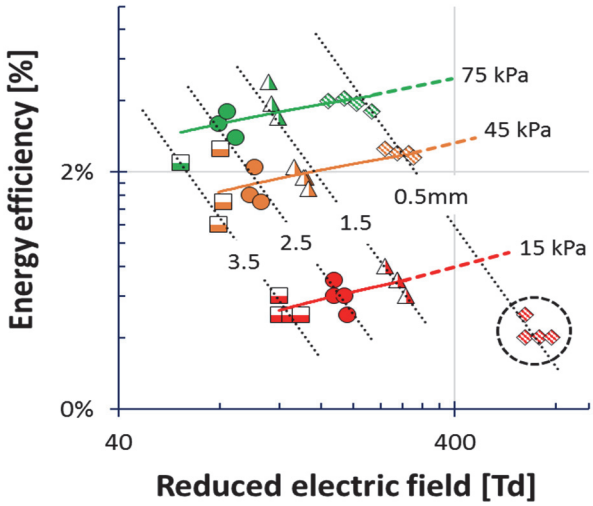

Fig. 3. Energy efficiency vs. Reduced electric field.

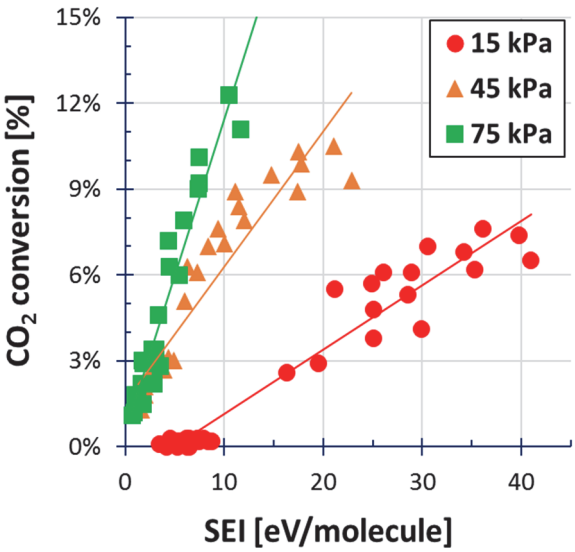

Fig. 4. CO_2 conversion as a function of *SEI*.

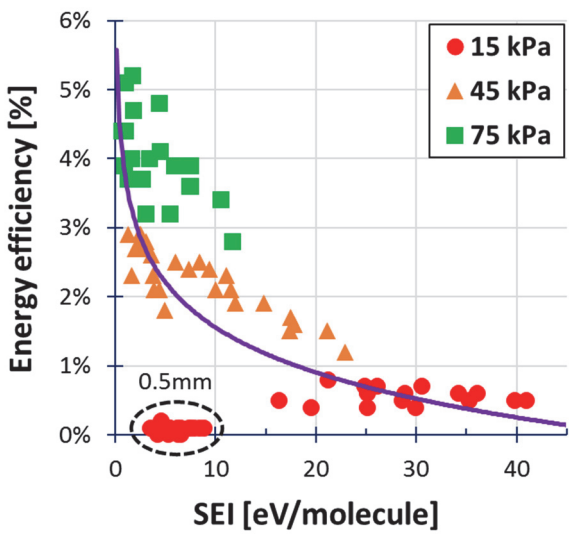

Fig. 5. Energy efficiency as a function of *SEI*.

On the increase *SEI*, CO_2 conversion is increasing, as illustrated in Fig. 4. Two reasons cause the increase of CO_2 conversion on *SEI*: (1) additional discharge power increases discharge current which enhances an interaction between electrons and CO_2 molecules. (2) Reducing the gas flow rate will increase the residence time of CO_2 molecules in the discharge region. Moreover, Fig. 4 also demonstrates a strong dependency of pressure on CO_2 activation to produce a distinct CO_2 conversion. Nonetheless, even though CO_2 conversion increased with increasing *SEI*, energy efficiency declined, as illustrated in Fig. 5. This result is logical given

the energy efficiency is proportional to the CO_2 conversion, yet inversely proportional to the *SEI*: there is a clear trade-off between CO_2 conversion and energy efficiency as a function of *SEI*. As discussed in Fig. 3, data obtained at 15 kPa and 0.5 mm gap are dislocated from the curve.

As for gas heating effect, Nozaki *et al*. have studied the heat and mass transport behavior in CH_4−fed DBD, and clarified the individual contribution of the steady-state average gas temperature increase and the transient gas heating by streamer formation [29]. Average gas temperature increases of the order of 10 K because less than 10% of total energy input is used for gas heating; ca. 90 % of heat is most likely dissipated to both electrodes. Therefore, the DBD reactor was exposed to an external cooling fan to ensure that the temperature of the ground electrode is near room temperature. Meanwhile, the internal high-voltage electrode was not equipped with a cooling device; therefore, the period of DBD operation was limited up to 3 minutes to avoid excessive electrode heating. The gas temperature within streamer increases temperately in the order of ΔT = 100 K. Unless the electrical properties of streamer change, such temperature increase is not influenced by the operating condition such as input power and gas flow rate [30]; note the average gas temperature varies by the operating conditions with the order of 10 K. We would like to point out that electron collision reaction is almost independent of gas temperature; therefore, CO_2 dissociation by direct electron impact reaction is considered to be independent in terms of gas heating. As for the vibrational ladder-climbing mechanism, ΔT = 100 K increase may promote V−T relaxation (vibrational deactivation) to some extent. Meanwhile, CO_2 conversion increases linearly with *SEI*, indicating V−T transition due to gas heating at higher *SEI* is a minor effect.

3.2 CO_2 dissociation mechanisms

Electron collision with CO_2 molecules may occur more rapidly in a high electric field because of a large population of the electron in the discharge region. However, Fig. 6 shows an opposite trend that CO_2 conversion declined on an increased electric field. To obtain a better understanding of electron impact reactions in the electric field from 60 to 700 Td, a numerical Boltzmann equation solver (BOLSIG+) was used. The electron and CO_2 collision cross section were adopted from Hayashi database [31] which is summarized in Table 2. The inelastic collision (momentum transfer collision) and the electron attachment collision are not included in Table 2. Fig. 7 shows the variation of reaction rate constants with respect to the reduced electric field. The mean electron energy is also provided.

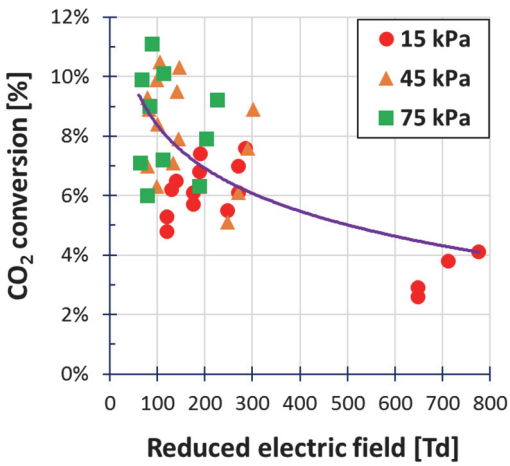

Fig. 6. CO_2 conversion as a function of a reduced electric field.

The CO_2 molecule has three fundamental vibration modes: symmetric stretching (1372 cm^{-1}), bending (640 cm^{-1}), and asymmetric stretching modes (2346 cm^{-1}). The most important vibration mode is the asymmetric stretching mode which leads to the dissociation of CO_2 via ladder-climbing mechanism as schematically shown in Fig. 8 [17]:

$$CO_2(n) + CO_2(m) \rightarrow CO_2(n+1) + CO_2(m-1) \rightarrow CO + O + CO_2(w) \quad (5)$$

Here, n, m, and w denote the asymmetric vibrational quantum number.

Table 2 The energy threshold of electron impact reactions of CO_2 obtained from Hayashi database [31].

Description	Reaction	Energy threshold (eV)	
Vibrational excitation	$CO_2 + e \rightarrow CO_2 + e$	0.083 eV	(R1)
	$CO_2 + e \rightarrow CO_2 + e$	0.172 eV	(R2)
	$CO_2 + e \rightarrow CO_2 + e$	0.291 eV	(R3)
	$CO_2 + e \rightarrow CO_2 + e$	0.36 eV	(R4)
	$CO_2 + e \rightarrow CO_2 + e$	2.5 eV	(R5)
Electronic excitation	$CO_2 + e \rightarrow CO_2^* + e$	5.7 eV	(R6)
	$CO_2 + e \rightarrow CO_2^* + e$	9.0 eV	(R7)
	$CO_2 + e \rightarrow CO_2^* + e$	11.0 eV	(R8)
Ionization	$CO_2 + e \rightarrow CO_2^+ + 2e$	13.7 eV	(R9)

The asymmetric vibrational CO_2 is produced via R3 in nonthermal plasma, showing the large rate constant from 60 to 700 Td. Multiple collisions between asymmetric vibrational CO_2 lead to the dissociation into CO and O (Eq. 5) when the quantum number exceeds v = 21 which corresponds to the CO_2 dissociation limit (5.52 eV) [32]. To ensure such high collision frequency, high-pressure nonthermal plasma such as DBD and gliding arc discharge is desired. Activation into the bending mode (R1) and the symmetric stretching mode (R2) are also strong, but excitation into these modes is not as important as asymmetric stretching mode for V−V energy transfer. In addition to fundamental vibration modes, another vibrational excitation, such as (R5), is possible in nonthermal plasma. The excitation level is about half of the dissociation limit which may imply a single collision between these molecules lead to CO_2 dissociation. However, the rate constant is an order of magnitude smaller than that of fundamental vibration modes; therefore, R5 is excluded from the dominant pathway.

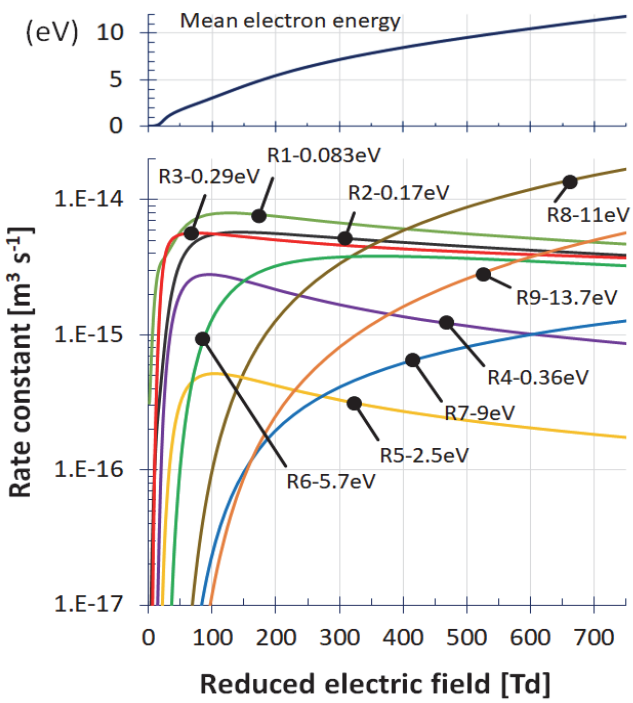

Fig. 7. Electron collision rate constants estimated by BOLSIG+ (version 03/2016).

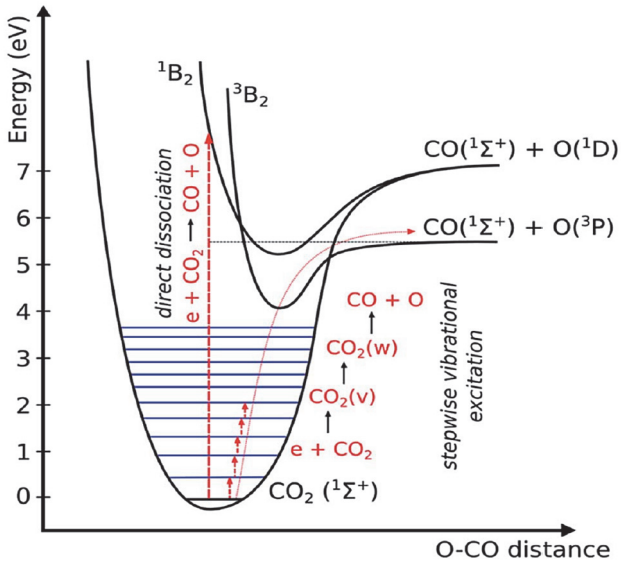

Fig. 8. Schematic diagram of vibrational and electronic levels of CO_2 molecule (reproduced from ref. [17] with permission from the Royal Society of Chemistry).

As the reduced electric field increases, the contribution of electronic excitation (R6) becomes the dominant pathway after 300 Td. Reaction (R8) also exhibits higher reaction rate compared to other electronic excitation reactions. In R6 and R8, CO_2 is excited into the electronic excitation potential (Fig. 8). The excitation energy is clearly larger than the CO_2 dissociation limit. The electronically excited CO_2 dissociates eventually into CO and O, but the excess energy fed into CO_2 is dissipated to the ambient as heat (energy loss). The vibrational ladder-climbing mechanism is more efficient than direct dissociation pathway because energy transfer between CO_2 (n) and CO_2 (m) occurs efficiently without excess energy transfer into the electronically excited state of CO_2. However, there is a trade-off between energy efficiency and CO_2 conversion as shown in Figs. 4–5: production of higher vibrational state (CO_2 (n+1)) inevitably accompanies deactivation of counter molecule (CO_2 (m-1)). Such trade-off relationship is observed in DBD, gliding arc discharge, and MW plasma as presented in the recent review paper [26].

Yamazaki *et al*. have performed a kinetic study of plasma-activated CO_2 dissociation using a low-pressure recombining hydrogen plasma [33]. They selected such unique plasma as extremely low-energy electron plasma source which is suitable for CO_2 vibrational activation and minimize inefficient direct dissociation process. Moreover, they performed the comprehensive in situ plasma diagnostics of the recombining plasma, showing electron density; 10^{18}–10^{19} m^{-3} and mean electron energy; 0.15–0.45 eV at 8.8 Pa. Because of low gas pressure and high electron density, vibrational ladder-climbing via multiple electron collision becomes the dominant pathway:

$$CO_2(n) + e = CO_2(n+1) + e \quad (6)$$

Unlike high-pressure nonthermal plasma such as DBD and gliding arc discharge, V–V energy transfer is inefficient in the low-pressure recombining plasma. However, the electron-induced ladder-climbing mechanism (Eq. 6) is possible, yielding the CO_2 conversion as high as 60%. Their study implicates the necessity of a new plasma source for efficient CO_2 splitting by electronic process: a low-energy and high-density electron plasma would break the limitation of the trade-off between CO_2 conversion and energy efficiency via an electron-induced ladder-climbing pathway.

4. Conclusion

CO_2 activation experiments were conducted at three pressures and four discharge gaps on a DBD reactor. Several principal parameters of DBD, such as pressure, specific energy input, and reduced electric field, were explored systematically. Moreover, the influence of the rate constant of electron impact reactions was investigated by electron Boltzmann equation solver (BOLSIG+).

An efficient CO_2 dissociation is possible by the vibrational ladder-climbing mechanism when the reduced electric field is small (< 300 Td) and high gas pressure (> 45 kPa) is ensured. Direct dissociation pathway would become dominant as the reduced electric field exceeds 300 Td. A low-pressure operation suppresses the ladder-climbing mechanism even if the reduced electric field is smaller than 300 Td. Meanwhile, the vibrational ladder-climbing shows the trade-off between energy efficiency and CO_2 conversion. Because one molecule gains vibrational energy via V−V energy transfer, meaning the counter molecule loses vibrational energy. To overcome such an obstacle, the electron-induced ladder-climbing mechanism would satisfy the higher energy efficiency and CO_2 conversion simultaneously. One possible approach is the low-pressure recombining hydrogen plasma proposed by Yamazaki *et al*. From the viewpoint of energy cost and scalability, a necessity of a new plasma source, which is equivalent to the hydrogen recombining plasma, is desired.

Acknowledgment

This project is supported by JST CREST (JPMJCR19R3). D.A. acknowledges financial support from the program of JICA Innovative Asia. Z.S. acknowledges financial support from the program of China Scholarships Council (201707040056).

References

[1] Neyts, E. C., Plasma-surface interactions in plasma catalysis, *Plasma Chem. Plasma Process*., Vol. 36 (1), pp. 185–212, Jan. 2016.

[2] Wang S., Zhang Y., Liu X., and Wang X., Enhancement of CO_2 conversion rate and conversion efficiency by homogeneous discharges, *Plasma Chem. Plasma Process*., Vol. 32 (5), pp. 979–989, Oct. 2012.

[3] Aerts R., Martens T., and Bogaerts A., Influence of vibrational states on CO_2 splitting by dielectric barrier discharges, *J. Phys. Chem. C*, Vol. 116 (44), pp. 23257–23273, Nov. 2012.

[4] Mei D., He Y.-L., Liu S., Yan J., and Tu X., Optimization of CO_2 conversion in a cylindrical dielectric barrier discharge reactor using design of experiments, *Plasma Process. Polym.*, Vol. 13 (5), pp. 544–556, May 2016.

[5] Kogelschatz U., Dielectric-barrier discharges: Their history, discharge physics, and industrial applications, *Plasma Chem. and Plasma Process.*, Vol. 23 (1). pp. 1–46, Mar-2003.

[6] Li J., Ma C., Zhu S., Yu F., Dai B., and Yang D., A Review of recent advances of dielectric barrier discharge plasma in catalysis, *Nanomaterials*, Vol. 9 (10), p. 1428, Oct. 2019.

[7] Firoozabadi E. A. and Hosseini S. M. H., Comparison of distinct discharge modes for ozone production in a novel DBD configuration with three flat electrodes, *IEEE Trans. Plasma Sci*., Vol. 47 (3), pp. 1562–1571, Mar. 2019.

[8] Eliasson B., Hirth M., and Kogelschatz U., Ozone synthesis from oxygen in dielectric barrier discharges, *J. Phys. D. Appl. Phys*., Vol. 20 (11), pp. 1421–1437, Nov. 1987.

[9] Ray D., Nepak D., Janampelli S., Gosha P. l, and Subrahmanyam C., Dry reforming of methane in DBD plasma over Ni-based catalysts: Influence of process conditions and support on performance and durability, *Energy Technol*., Vol. 7 (4), p. 1801008, Apr. 2019.

[10] Kameshim S., Tamura K., Ishibashi Y., and Nozaki T., Pulsed dry methane reforming in plasma-enhanced catalytic reaction, *Catal. Today*, Vol. 256 (Part 1), pp. 67–75, Nov. 2015.

[11] Sheng Z., Sakata K., Watanabe Y., Kameshima S., Kim H.H., Yao, S. and Nozaki T., Factors determining synergism in plasma catalysis of biogas at reduced pressure, *J. Phys. D. Appl. Phys*., Vol. 52 (41), p. 414002, Oct. 2019.

[12] Niu G., Qin Y., Li W., and Duan Y., Investigation of CO_2 splitting process under atmospheric pressure using multi-electrode cylindrical DBD Plasma reactor, *Plasma Chem. Plasma Process.*, Vol. 39 (4), pp. 809–824, Jul. 2019.

[13] Mei D. and Tu X., Conversion of CO_2 in a cylindrical dielectric barrier discharge reactor: Effects of plasma processing parameters and reactor design, *J. CO_2 Util*., Vol. 19, pp. 68–78, May 2017.

[14] Ozkan A., Dufour T., Silva T., Britun N., Snyders R., Bogaerts A., and Reniers F., The influence of power and frequency on the filamentary behavior of a flowing DBD—application to the splitting of CO_2, *Plasma Sources Sci. Technol*., Vol. 25 (2), p. 025013, Apr. 2016.

[15] Rouwenhorst K.H.R., Kim H.H., and Lefferts L., Vibrationally excited activation of N_2 in plasma-enhanced catalytic ammonia synthesis: A kinetic analysis, *ACS Sustain. Chem. Eng*., Vol. 7 (20), pp. 17515–17522, Oct. 2019.

[16] Patil B. S., Wang Q., Hessel V., and Lang J., Plasma N_2-fixation: 1900–2014, *Catal. Today*, Vol. 256 (1), pp. 49–66, Nov. 2015.

[17] Bogaerts A., Kozák T., Laer K. van, and Snoeckx R., Plasma-based conversion of CO_2: Current status and future challenges, *Faraday Discuss*., Vol. 183, pp. 217–232, 2015.

[18] Qin Y., Niu G., Wang X., Luo D., and Duan Y., Status of CO_2 conversion using microwave plasma, *J. CO_2 Util.*, Vol. 28, pp. 283–291, Dec. 2018.
[19] Rusanov V.D., Fridman A.A., and Sholin G.V., The physics of a chemically active plasma with nonequilibrium vibrational excitation of molecules, *Sov. Phys. Uspekhi*, Vol. 24 (6), pp. 447–474, Jun. 1981.
[20] Berthelot A., and Bogaerts A., Modeling of CO_2 splitting in a microwave plasma: How to improve the conversion and energy efficiency, *J. Phys. Chem. C*, Vol. 121 (15), pp. 8236–8251, Apr. 2017.
[21] Fridman A., Plasma Chemistry. Cambridge University Press, 2008.
[22] Fridman A. and Kennedy L. A., Plasma Physics and Engineering. Taylor and Francis Group, 2011.
[23] Wang W., Berthelot A., Kolev S., Tu X., and Bogaerts A., CO_2 conversion in a gliding arc plasma: 1D cylindrical discharge model, *Plasma Sources Sci. Technol.*, Vol. 25 (6), p. 065012, Oct. 2016.
[24] Nunnally T., Gutsol K., Rabinovich A., Fridman A., Gutsol A., and Kemoun A., Dissociation of CO_2 in a low current gliding arc plasmatron, *J. Phys. D. Appl. Phys.*, Vol. 44 (27), p. 274009, Jul. 2011.
[25] Zhang H., Li L., Li X., Wang W., Yan J., and Tu X., Warm plasma activation of CO_2 in a rotating gliding arc discharge reactor, *J. CO_2 Util.*, Vol. 27, no. September, pp. 472–479, Oct. 2018.
[26] Snoeckx R. and Bogaerts A., Plasma technology – a novel solution for CO_2 conversion?, *Chem. Soc. Rev.*, Vol. 46 (19), pp. 5805–5863, 2017.
[27] Uytdenhouwe Y.n, Alphen S. Van, Michielsen I., Meynen V., Cool P., and Bogaerts A., A packed-bed DBD micro plasma reactor for CO_2 dissociation: Does size matter?, *Chem. Eng. J.*, Vol. 348, pp. 557–568, Sep. 2018.
[28] Sheng Z., Kameshima S., Yao S., and Nozaki T., Oxidation behavior of Ni/Al_2O_3 catalyst in nonthermal plasma-enabled catalysis, *J. Phys. D. Appl. Phys.*, Vol. 51 (44), p. 445205, Nov. 2018.
[29] Nozaki T., Miyazaki Y., Unno Y., and Okazaki K., Energy distribution and heat transfer mechanisms in atmospheric pressure non-equilibrium plasmas, *J. Phys. D. Appl. Phys.*, Vol. 34 (23), pp. 3383–3390, Dec. 2001.
[30] Nozaki T., Unno Y., and Okazaki K., Thermal structure of atmospheric pressure non-equilibrium plasmas, *Plasma Sources Sci. Technol.*, Vol. 11 (4), pp. 431–438, Nov. 2002.
[31] Hayashi database. [Online]. Available: www.lxcat.net. [Accessed: 31-Jul-2019].
[32] Kozák T. and Bogaerts A., Splitting of CO_2 by vibrational excitation in non-equilibrium plasmas: a reaction kinetics model, *Plasma Sources Sci. Technol.*, Vol. 23 (4), p. 045004, Jun. 2014.
[33] Yamazaki M., Nishiyama S., and Sasaki K., Decomposition of carbon dioxide by recombining hydrogen plasma with ultralow electron temperature, *Appl. Phys. Express*, Vol. 11 (6), p. 066202, Jun. 2018.